Available online at www.sciencedirect.com
ScienceDirect
Separation and Purification Technology 60 (2008) 230–236
Separation Purification Technology
www.elsevier.com/locate/seppur

Investigation of slowing-down and speeding-up effects in binary mixture permeation across SAPO-34 and MFI membranes

R. Krishna [a,*], Shiguang Li [b], Jasper M. van Baten [a], John L. Falconer [b], Richard D. Noble [b]

[a] *Van't Hoff Institute for Molecular Sciences, University of Amsterdam, Nieuwe Achtergracht 166, 1018 WV, Amsterdam, The Netherlands*
[b] *Department of Chemical and Biological Engineering, University of Colorado, Boulder, CO 80309-0424, USA*

Received 30 March 2007; received in revised form 10 August 2007; accepted 13 August 2007

Abstract

Permeation experiments for Ar/CH_4 and CO_2/H_2 mixtures across a SAPO-34 membrane were performed with the objective of highlighting their distinct diffusion characteristics. For the Ar/CH_4 mixture, the effective transport coefficients of the individual components in the mixture were found to be practically the same as those obtained from unary permeation experiments, when compared at the same total loading at the upstream face of the membrane. There is no speeding-up of the tardier CH_4. Only at the high loadings is there evidence of a small, about 10%, slowing-down of the more mobile Ar.

A different picture emerges for permeation of CO_2/H_2 mixtures across SAPO-34 membrane. While the transport coefficient of CO_2 is practically identical to those obtained from unary experiments, there is a significant slowing-down of the more mobile H_2. At the highest loading, the transport coefficient of H_2 is about a third of the value of the pure component.

Permeation of CO_2/CH_4 mixtures across an MFI membrane showed that there is a significant slowing-down of the more mobile CH_4 with concomitant speeding-up of the tardier CO_2.

The incorporation of the Vignes interpolation formula for the exchange coefficient $Đ_{12}$ in the Maxwell–Stefan equations does not adequately reflect the slowing-down and speeding-up phenomena for either SAPO-34 or MFI membranes.

Keywords: Zeolite membrane; SAPO-34; MFI; Maxwell–Stefan diffusivity; Loading dependence; Correlation effects; Mixture diffusion

1. Introduction

There is considerable interest in the use of zeolite membranes for separating gaseous mixtures such as CO_2/CH_4, CO_2/N_2, CH_4/N_2, O_2/N_2, and CO_2/H_2 [1–3]. The membrane permeation selectivity is dictated both by the adsorption and diffusion behaviors in the mixture. Molecular dynamics simulations show that due to correlation effects the mobility of a given species is influenced by the presence of other species [4–7]. Often the more mobile species gets slowed down, and the tardier species gets speeded up; the extent of slowing-down and speeding-up has been found to depend on the particular zeolite [8]. For design of membrane separation units it is important to model correlation effects in a manner that can be incorporated into process design equations. For this purpose, the Maxwell–Stefan (M–S) are widely used in practice [8,9] to model n-component mixture diffusion:

$$-\rho\frac{\theta_i}{RT}\frac{\mathrm{d}\mu_i}{\mathrm{d}x}=\sum_{\substack{j=1\\ j\neq i}}^{n}\frac{q_jN_i-q_iN_j}{q_{i,\mathrm{sat}}q_{j,\mathrm{sat}}Đ_{ij}}+\frac{N_i}{q_{i,\mathrm{sat}}Đ_i},\quad i=1,2,\ldots,n \tag{1}$$

In Eq. (1) the fractional occupancies θ_i are defined by

$$\theta_i\equiv\frac{q_i}{q_{i,\mathrm{sat}}},\quad i=1,2,\ldots,n \tag{2}$$

Within the framework of the M–S formulation correlation effects are embodied in the exchange coefficients $Đ_{ij}$ that quantify the extent of slowing-down and speeding-up. Conformity with the Onsager reciprocal relations demands that

$$q_{j,\mathrm{sat}}Đ_{ij}=q_{i,\mathrm{sat}}Đ_{ji} \tag{3}$$

For equal saturation capacities we have $Đ_{ij}=Đ_{ji}$ as used in early publications [10]. On the basis of MD simulations we note that

* Corresponding author. Tel.: +31 20 5257007; fax: +31 20 5255604.
E-mail address: r.krishna@uva.nl (R. Krishna).

1383-5866/$ – see front matter © 2007 Elsevier B.V. All rights reserved.
doi:10.1016/j.seppur.2007.08.012

Nomenclature

$Đ_i$	Maxwell–Stefan diffusivity of species i ($m^2\ s^{-1}$)
$Đ_i(0)$	zero-loading M–S diffusivity of species i ($m^2\ s^{-1}$)
$Đ_{ii}$	self-exchange diffusivity ($m^2\ s^{-1}$)
$Đ_{ij}$	binary exchange diffusivity ($m^2\ s^{-1}$)
n	number of species in mixture
N_i	molar flux of species i across membrane ($mol\ m^{-2}\ s^{-1}$)
q	total mixture loading ($mol\ kg^{-1}$)
q_i	molar loading of species i ($mol\ kg^{-1}$)
$q_{i,sat}$	saturation loading of species i ($mol\ kg^{-1}$)
R	gas constant ($8.314\ J\ mol^{-1}\ K^{-1}$)
T	absolute temperature (K)
x	spatial distance (m)

Greek letters

Γ_{ij}	thermodynamic factors
δ	thickness of zeolite membrane (m)
Δ_{ij}	matrix with elements defined by Eqs. (6) and (7) ($m^2\ s^{-1}$)
θ_i	fractional occupancy of component i
μ_i	molar chemical potential ($J\ mol^{-1}$)
ρ	density of zeolite ($kg\ m^{-3}$)

Subscripts

i, j	referring to species i and j
sat	referring to saturation conditions
up	referring to conditions at upstream face of membrane

the ratio $Đ_{ij}/Đ_i$ usually lie in the range of 0.1–3, depending on the particular guest–host combination [4,8,11].

The gradient of the chemical potentials in Eq. (1) can be related to the gradients in the loadings by defining an $n \times n$ matrix of thermodynamic factors $[\Gamma]$:

$$\frac{q_i}{RT}\frac{d\mu_i}{dx} = \sum_{j=1}^{n}\Gamma_{ij}\frac{dq_j}{dx}, \qquad \Gamma_{ij} \equiv \frac{q_i}{f_i}\frac{\partial f_i}{\partial q_j}, \quad i, j = 1, \ldots, n \tag{4}$$

The elements Γ_{ij} in Eq. (4) can be estimated using the ideal adsorbed solution theory (IAST) of Myers and Prausnitz [12] and the fits of the pure component isotherm data. The fluxes N_i are explicitly related to the gradients in the loading by the n dimensional matrix relations:

$$N = -\rho[\Delta][\Gamma]\frac{d(q)}{dx} \tag{5}$$

For a binary mixture, $n = 2$, the diagonal elements Δ_{11} and Δ_{22} can be written explicitly as follows

$$\Delta_{11} = \frac{Đ_1}{1 + ((\theta_2/(Đ_{12}/Đ_1))/(1 + (\theta_1/(Đ_{21}/Đ_2))))},$$
$$\Delta_{22} = \frac{Đ_2}{1 + ((\theta_1/(Đ_{21}/Đ_2))/(1 + (\theta_2/(Đ_{12}/Đ_1))))} \tag{6}$$

The denominators in Eq. (6) quantify the slowing-down effects. Clearly, the slowing-down will be significant only at high occupancies θ_i. To illustrate the slowing-down effects we present in Fig. 1a MD simulations of Δ_{ii} for CO_2 (1) and CH_4 (2) mixture in MFI zeolite at a total loading $q_1 + q_2 = 2.6\ mol\ kg^{-1}$ and varying composition of the two species. In MFI, CO_2 is the tardier species, and with increasing proportion of CO_2 there is a strong decrease in the Δ_{22} of CH_4. The M–S diffusivity of CO_2 and Δ_{11}, is also lower in the mixture than the pure component value, but this reduction is far less severe than that of the more mobile CH_4. It is interesting to note that for mixtures wherein the mole fraction of CO_2 in the adsorbed phase is higher than 0.6, mobility-reversal takes place, and $\Delta_{11} > \Delta_{22}$.

The cross-coefficients of Δ_{12} and Δ_{21} are

$$\Delta_{12} = \frac{(q_{1,sat}/q_{2,sat})(\theta_1/(Đ_{12}/Đ_1))Đ_2}{1 + ((\theta_1/(Đ_{21}/Đ_2)) + (\theta_2/(Đ_{12}/Đ_1)))},$$
$$\Delta_{21} = \frac{(q_{2,sat}/q_{1,sat})(\theta_2/(Đ_{21}/Đ_2))Đ_1}{1 + ((\theta_1/(Đ_{21}/Đ_2)) + (\theta_2/(Đ_{12}/Đ_1)))} \tag{7}$$

There are only three independent coefficients Δ_{ij}; the cross-coefficients are inter-related by $q_2\Delta_{12} = q_1\Delta_{21}$ as a consequence of the Onsager reciprocal relations; this relation was incorrectly printed earlier [4,5]. Speeding-up is caused by cross-coefficients with finite and significant values. A tardy species 1 will be speeded-up by the more mobile species 2 due to a finite cross-term Δ_{12}. Due to the occurrence of the occupancies θ_i in the numerator in Eq. (7), it is clear that speeding-up is only effective at high occupancies. A further requirement of a significant speeding-up of species 1 is that the ratio of the driving force for component 2 to that of component 1, i.e.:

$$\frac{(\Gamma_{22}(dq_2/dx)) + (\Gamma_{21}(dq_1/dx))}{(\Gamma_{11}(dq_1/dx)) + (\Gamma_{12}(dq_2/dx))} \gg 1 \tag{8}$$

should exceed unity to a significant extent. This ratio will be significantly larger than unity only when species 2 is much more strongly adsorbed than species 1. The combination of the two requirements: (a) higher mobility of species 2 and (b) higher adsorption strength for species 2 is rare and for this reason speeding-up is also rare. It is more common to find that the more mobile species is also more poorly adsorbed; speeding-up will usually be of negligible importance.

For zeolites that consist of cages, separated by narrow windows, such as CHA, DDR, and LTA it has been argued that inter-cage hopping of molecules occur practically independent of one another [13]. For these types of zeolites it has been suggested that the approximation $(Đ_{ij}/Đ_i) \to \infty$ holds [13]; consequently the cross-coefficients Δ_{ij} vanish, and Eq. (1) simplifies to yield a set of uncoupled equations:

$$N_i = -\rho Đ_i\frac{q_i}{RT}\frac{d\mu_i}{dx}, \quad i = 1, 2, \ldots, n \tag{9}$$

In the early work of Habgood [14], Eq. (9) was used to describe N_2/CH_4 mixture diffusion in LTA zeolite and for this reason we shall refer to this simplified variant of the M–S equations as the Habgood model.

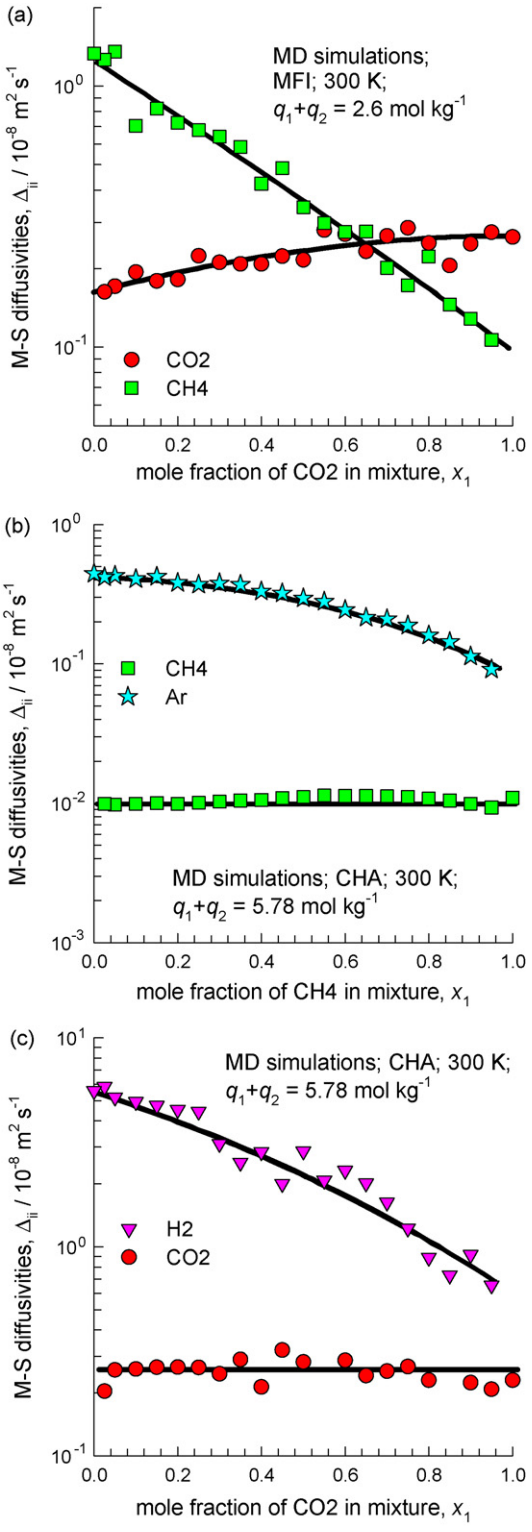

Fig. 1. MD simulations of M–S diffusivities of Δ_{ii} in (a) CO_2/CH_4 mixture in MFI, (b) Ar/CH_4 mixture in CHA, and (c) CO_2/H_2 mixture in CHA. The MD simulation methodology is as described in our earlier publication [8]. Note that the Δ_{22} of CH_4 in CHA were too low to be determined accurately; the presented data are the self-diffusivity, that is more accurately determined.

For binary mixture permeation across a zeolite membrane of thickness δ, we may integrate Eq. (9) to obtain

$$N_i = \frac{\rho}{\delta}\int_{\text{upstream}}^{\text{downstream}} Đ_i \sum_{j=1}^{n}\left(\Gamma_{ij}\frac{\mathrm{d}q_j}{\mathrm{d}x}\right)\mathrm{d}x, \quad i = 1, 2 \tag{10}$$

The details of the numerical procedures for calculation of the fluxes are described in earlier work [9,15]. In carrying out the integration the loading dependence of $Đ_i$ needs to be properly accounted for, as discussed in Supplementary data.

In recent work, Li et al. [3] found that Eq. (10) provided a good quantitative estimation of the permeation fluxes for CO_2/CH_4, CO_2/N_2, CH_4/N_2, and $CO_2/CH_4/N_2$ mixtures across a SAPO-34 membrane using only pure component adsorption and transport information. SAPO-34 is an isotype of CHA zeolite and consists of cages separated by 3.8 Å sized windows and inter-cage hops of molecules do not appear to be correlated for the range of pressures used in the experiments. For permeation of binary mixtures H_2/CH_4, H_2/N_2, and H_2/CO, Li et al. [3] found that the Habgood model provided a reasonably good, but not perfect match with the experiments. There was evidence of a slight slowing-down of mobile H_2, with concomitant, small, speeding-up of the tardier CH_4, N_2, or CO species in the three binary mixtures considered.

Recent MD simulations [8] have shown that Eq. (9) is a reasonable approximation provided that the mixture loadings are not too high and the total occupancy in the zeolite is lower than about 0.4. Furthermore, it has been shown that for weakly confined species such as Ne and H_2, the Habgood approximation (9) breaks down even for CHA, DDR, and LTA zeolites. To underline this we have presented in Fig. 1b and c MD simulations results of Δ_{ii} for Ar/CH_4 and CO_2/H_2 mixtures in CHA as a function of mixture composition. The total loading $q_1 + q_2$ was chosen to be 5.8 mol kg^{-1} yielding occupancies in the mixture of about 0.5–0.6, a value that is high enough to test the Habgood approximation in a stringent manner. For the Ar/CH_4 mixture (cf. Fig. 1b), there is a threefold reduction in the diffusivity if Ar is reduced when the fraction of CH_4 in the mixture is increased from 0 to 1. For the CO_2/H_2 mixture (cf. Fig. 1c), the reduction in the diffusivity of H_2 is nearly 10-fold when the fraction of CO_2 in the mixture is increased from 0 to 1. For both mixtures we note that there is practically no speeding-up of the tardier species, CH_4 and CO_2, in the two respective mixtures. The significant reduction in the diffusivity of H_2 is due to correlation effects as emphasized earlier [8].

The first major objective of the present work is to subject the applicability of the Habgood model for mixture permeation across SAPO-34 membrane to further stringent testing by carrying out experiments with Ar/CH_4 and CO_2/H_2 mixtures. We aim to demonstrate that while the Habgood model is a good approximation for low mixture loadings within the zeolite, it gets progressively worse at higher loadings, especially for a small species such as H_2 that is weakly confined within the zeolite. The strong reduction in the H_2 diffusivity in CO_2/H_2 mixtures as witnessed in Fig. 1c will be tested. The experiments were carried out using the same SAPO-34 membrane as described in our previous study [3].

MD simulations have shown that correlation effects are particularly strong within the intersecting channel structures of MFI zeolite [8]; the second major objective is to verify this by carrying out CO_2/CH_4 permeation experiments across an MFI membrane. We aim to show that in this case we have both significant slowing-down and speeding-up effects. The details of MFI membrane synthesis, characterization, and measurement procedures along with the experimental data in tabular form have been given in the Supplementary data accompanying this publication. These data, combined with our published mixture permeation data [3], are discussed below.

2. Permeation across SAPO-34 membrane

Comparison of the experimental fluxes with the estimations of N_i using Eq. (10) is presented in Fig. 2 for (a) Ar/CH_4 and (b) CO_2/H_2 mixtures. In the model calculations the mixture loadings were estimated from the IAST using the pure component isotherm fits as reported in earlier work [3]. The Reed and Ehrlich model was used to describe the dependence of the unary transport coefficients $\rho Đ_i/\delta$ on occupancy, as outlined earlier [3]; see Supplementary data accompanying this publication. We note that Habgood model provides good estimates of each of the component fluxes for the Ar/CH_4 mixture. At the highest pressures, the Habgood model appears to slightly over-predict the flux of the more mobile Ar. For the CO_2/H_2 mixture, while the predictions of the CO_2 flux are very good, the Habgood model severely over-predicts the H_2 flux.

To rationalize these observations we backed out the transport diffusivity $\rho Đ_i/\delta$ as a function of the total upstream loading, $q_{up} = q_{1,up} + q_{2,up}$, for the eight sets of binary mixture permeation experiments (the previously published set for CO_2/CH_4, CO_2/N_2, N_2/CH_4, CH_4/H_2, CO/H_2, and N_2/H_2 along with the two new sets for Ar/CH_4 and CO_2/H_2 from current work) using

$$\frac{\rho Đ_i}{\delta} = \frac{N_i}{\int_{\text{upstream}}^{\text{downstream}} \sum_{j=1}^{n} \left(\Gamma_{ij} \frac{dq_j}{dx} \right) dx}, \quad i = 1, 2 \tag{11}$$

The results are presented in Fig. 3a–d along with the backed out transport coefficients from unary permeation experiments. It must be emphasized that the backed out transport diffusivities $\rho Đ_i/\delta$ are effective and integral parameters that will correspond with those obtained from unary experiments only when the exchange coefficients are large, i.e. $(Đ_{ij}/Đ_i) \to \infty$. A further point to be emphasized in Fig 3 is that the $\rho Đ_i/\delta$ are loading dependent.

From Fig. 3a we note that as q_{up} increases, the $\rho Đ_i/\delta$ for Ar progressively falls below the pure component value. It appears that the slowing-down of Ar becomes progressively more important at increased loadings. A molecular interpretation is that inter-cage hops become increasingly correlated as the loading increases. In the M–S framework, the slowing-down of Ar (species 1) is due to the term $1 + ((\theta_2/(Đ_{12}/Đ_1))/(1 + \theta_1/(Đ_{21}/Đ_2)))$ in Eq. (6) becoming increasingly large due to the much more strongly adsorbed CH_4, species 2 with $\theta_2 \gg \theta_1$. The predictions of the Habgood model become progressively worse with increased loadings. Nevertheless, the deviations between experimental fluxes and model remain below 10% as witnessed in Fig. 2a.

Let us consider the transport coefficient for CH_4, the tardiest of all species in the SAPO-34 experiments (see Fig. 3b). The value of $(\rho Đ_i/\delta)$ for CH_4 is practically the same whether it is present on its own or in the company of CO_2, Ar, or N_2. The results of Figs. 3a and b are in qualitative agreement with the MD simulation results in Fig. 1b for CHA.

We turn now to the transport coefficient of H_2, the most mobile species in the SAPO-34 experiments conducted. The pure component value of $\rho Đ_i/\delta$ lies in the narrow range of 0.26–0.3 kg m^{-2} s^{-1} (see Fig. 3c). H_2 has a low adsorption strength and the q_{up} value is less that 1.8 mol kg^{-1}. As the loading increases correlation effects increasingly influence intercage hopping of H_2, leading to a lowering in the effective transport coefficient in the mixture. The extent of lowering of effective transport coefficient for H_2 (species 2) depends on the term $1 + ((\theta_1/(Đ_{21}/Đ_2))/(1 + (\theta_2/(Đ_{12}/Đ_1))))$ in Eq. (6) and will increase with increased value of θ_1, the occupancy of the

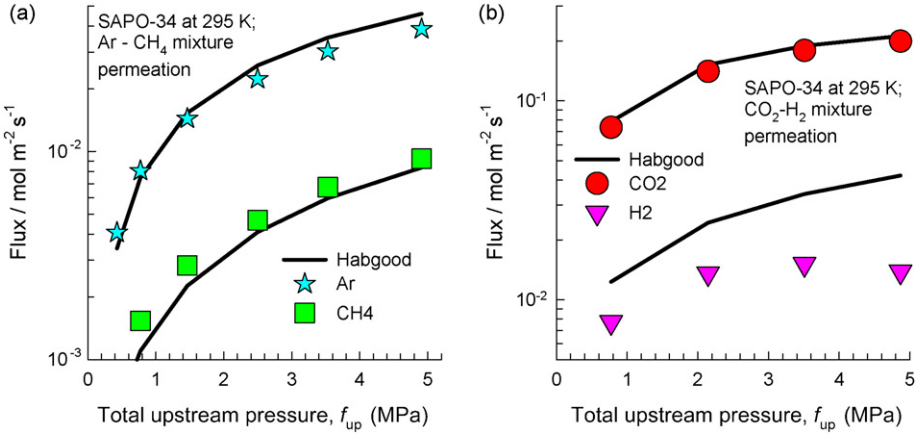

Fig. 2. Fluxes for (a) Ar/CH_4 and (b) CO_2/H_2 mixture permeation across SAPO-34 membrane as function of the upstream total pressure, f_{up}. The continuous solid lines represent the calculations by numerical solution of Eq. (10).

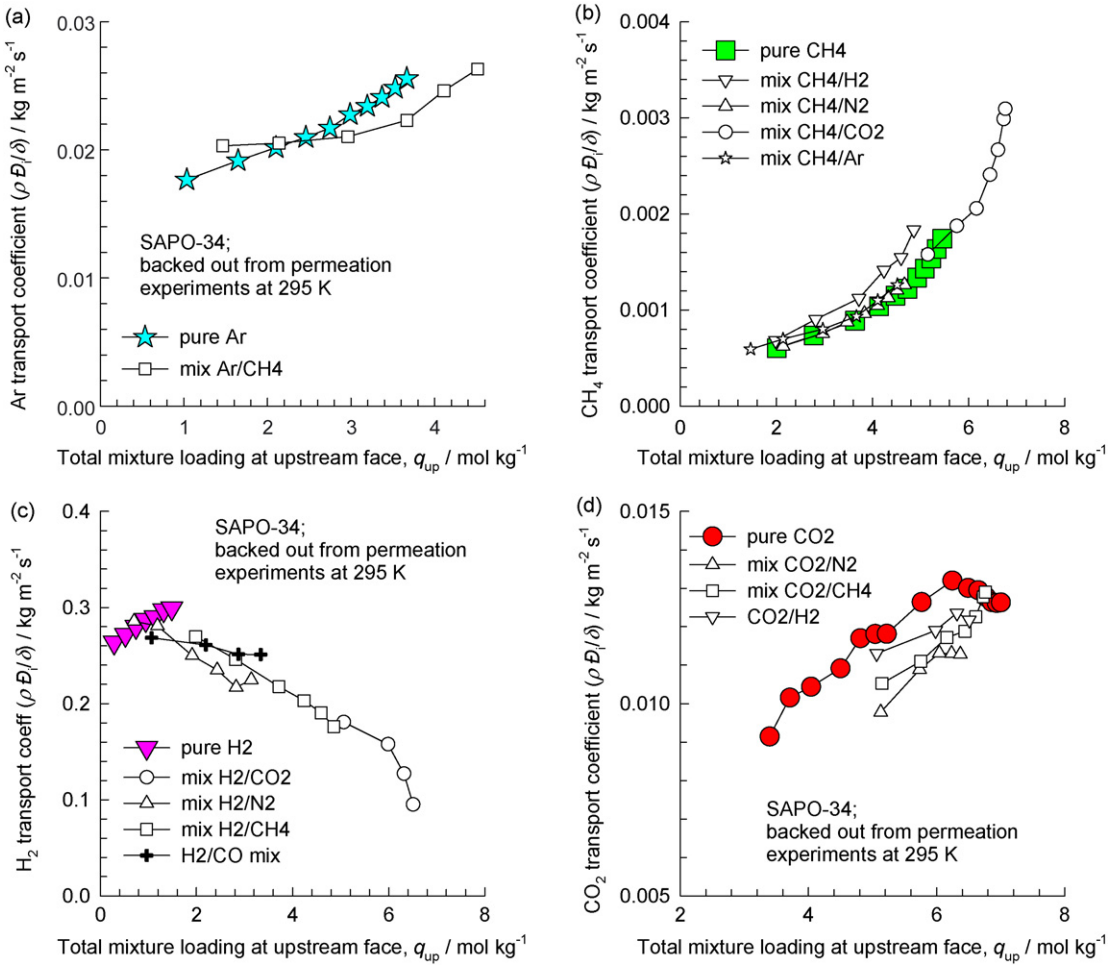

Fig. 3. Transport coefficients, $\rho Đ_i/\delta$, of (a) Ar, (b) CH_4, (c) H_2, and (d) CO_2, backed out from unary and binary permeation data for SAPO-34 membrane.

more strongly adsorbed species in the mixture. The adsorption strengths of N_2, CO, and CH_4 are significantly lower than that of CO_2 and the value of q_{up} for CH_4/H_2, CO/H_2 and N_2/H_2 mixtures is below 4 mol kg^{-1} for the range of upstream pressures used in the experiments. For these three mixtures, the reduction in the effective transport coefficient $\rho Đ_i/\delta$ for H_2 is smaller than 40%, leading us to conclude in earlier work that the Habgood model provides a reasonably good, though not perfect, match with experiments for CH_4/H_2, CO/H_2, and N_2/H_2 mixture permeation [3]. The situation is different for CO_2/H_2 mixtures; due to the considerably stronger adsorption strength of CO_2 the total loading q_{up} increases to values of 6.4 mol kg^{-1}, corresponding to $\theta_1 \approx 0.8$, and at the highest q_{up} the value of $\rho Đ_i/\delta$ for H_2 is about a third of the value of the pure component. The Habgood model does not adequately estimate the H_2 flux in the mixture, as it is evidenced in Fig. 2b. The results of Fig. 3c and d are in qualitative agreement with the MD simulation results in Fig. 1b and c for CHA.

We now examine whether the re-instatement of a finite exchange coefficient $Đ_{12}$ in the M–S Eq. (1) improves the predictions of CO_2/H_2 mixture permeation fluxes. The proper estimation of $Đ_{12}$ remains an issue. Use of the Vignes interpolation formula suggested earlier [9]:

$$Đ_{12} = [Đ_1]^{q_1/(q_1+q_2)}[Đ_2]^{q_2/(q_1+q_2)} \tag{12}$$

results in severe under prediction of H_2 fluxes (see Fig. 4). Eq. (12) anticipates too strong a correlation effect on H_2 diffusion in the mixture. The CO_2 flux appears to be insensitive to the inclusion, or not, of the $Đ_{12}$. The reasons for this insensitivity are twofold. First, since H_2 (2) is so poorly adsorbed compared to CO_2 (1), $\theta_2 \ll \theta_1$ and there is no slowing-down effect of cf. Eq. (6). Secondly, $(\Gamma_{22}(dq_2/dx) + \Gamma_{22}(dq_1/dx))/(\Gamma_{11}(dq_1/dx) + \Gamma_{12}(dq_2/dx)) \ll 1$, and consequently there is no speeding-up due to a finite cross-term Δ_{12}. Generally speaking, if one species is significantly more strongly adsorbed than its partner, its flux will hardly be influenced by correlation effects. To underline this further, we have presented in Fig. 3d the transport coefficient data for pure CO_2 along with those in a variety of binary mixtures. There is less than 20% influence of the presence of partner molecules on the transport coefficient of CO_2. Conversely, a poorly adsorbed species is affected significantly by its partner. For all eight binary mixtures investigated, the predictions of the CO_2 fluxes are good; this is because CO_2 has the strongest adsorption

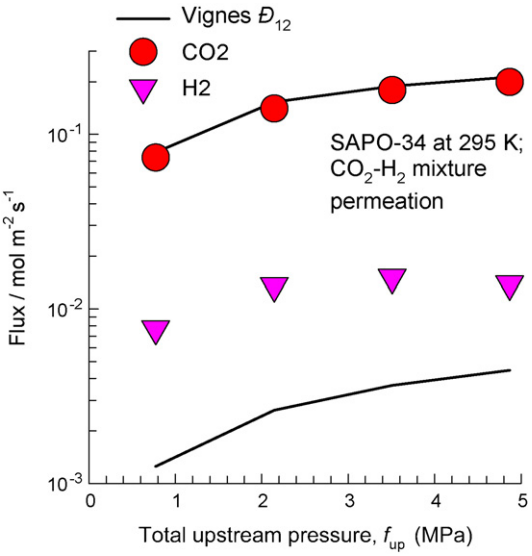

Fig. 4. Permeation fluxes for binary CO_2/H_2 mixtures across SAPO-34 membrane as function of the upstream total pressure, f_{up}. The continuous solid lines represent the calculations by numerical solution of Eq. (1) with $Đ_{12}$ estimated using the Vignes interpolation formula of Eq. (12).

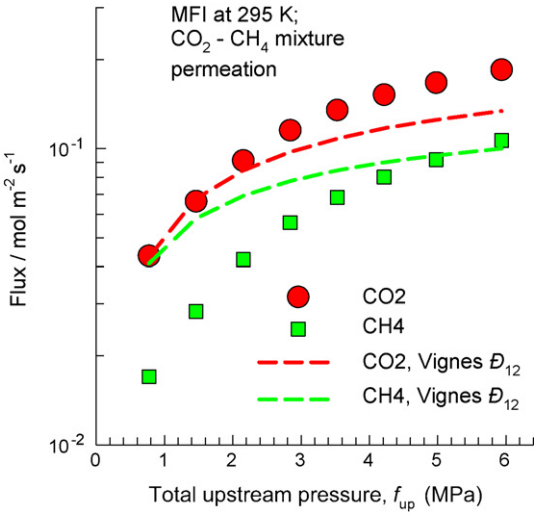

Fig. 6. Permeation fluxes for binary CO_2/CH_4 mixture across MFI membrane as function of the upstream total pressure, f_{up}. The continuous and dashed solid lines represent the calculations by numerical solution of Eq. (1) with $Đ_{12}$ estimated using the Vignes interpolation formula of Eq. (12).

strength and consequently the highest driving force and fluxes.

3. Permeation across MFI membrane

Fig. 5 compares the transport coefficients, $\rho Đ_i/\delta$ for MFI membrane backed out from unary and binary permeation of CO_2/CH_4. For the binary mixture experiments the $\rho Đ_i/\delta$ were backed out using Eq. (11). The IAST was used for calculation of mixture adsorption using the pure component three-site Langmuir fits presented in earlier work [11]. The first point to note is that the pure component $\rho Đ_i/\delta$ of CH_4 is higher than that of CO_2. This is reverse of the hierarchy for SAPO-34 membrane [3], but in line with the hierarchy obtained from MD simulation

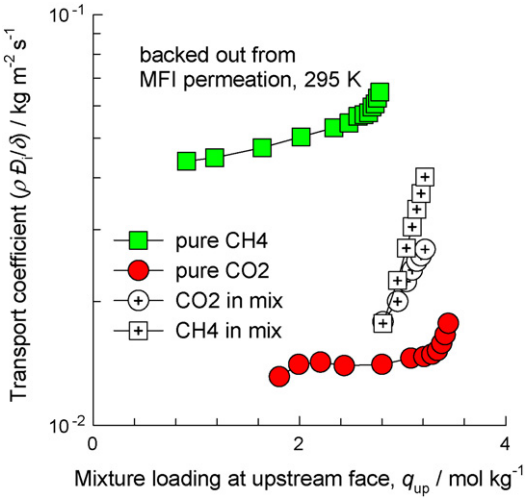

Fig. 5. Comparison of transport coefficients, $\rho Đ_i/\delta$, for MFI membrane backed out from unary permeation and binary mixtures containing CO_2/CH_4.

results for diffusion in MFI [8,13]; see also Fig. 1a CO_2 is a longer, more slender, molecule than CH_4. Within the channels of MFI the length of the molecule has an adverse influence on its diffusivity. When the transport coefficients in the mixture are compared with the corresponding unary values, we note that there is a strong reduction in the mobility of CH_4, with concomitant speeding-up of CO_2. It appears that in the mixture the two components have practically the same $\rho Đ_i/\delta$. Clearly, correlation effects are strong within the intersecting channel structure of MFI zeolite and the Habgood model will be inadequate for flux estimation purposes. Use of the Vignes interpolation formula (12) leads to the flux predictions that are poor for both components; see Fig. 6. At low upstream pressures, the flux of CH_4 is severely over-predicted; the slowing-down of the more mobile CH_4 is stronger than anticipated by the Vignes estimation of $Đ_{12}$. At high upstream pressures, the flux of CO_2 is severely under-predicted; the speeding-up of CO_2 is stronger than anticipated by the Vignes estimation of $Đ_{12}$. This conclusion regarding the limitation of the Vignes interpolation formula was also highlighted by Yu et al. [16] in the context of transient permeation modeling of polar organic molecules across a MFI membrane.

In this connection it must be remarked that the interpolation formula suggested on the basis of MD simulation results [4,17]:

$$q_{2,\mathrm{sat}}Đ_{12} = [q_{2,\mathrm{sat}}Đ_{11}]^{q_1(q_1+q_2)}[q_{1,\mathrm{sat}}Đ_{22}]^{q_2(q_1+q_2)} = q_{1,\mathrm{sat}}Đ_{21} \tag{13}$$

is difficult to employ in practice as it is not possible to determine the self-exchange coefficients $Đ_{11}$ and $Đ_{22}$ from experimental permeation data alone. For this purpose we need information on pure component self-diffusivities, along with M–S diffusivities; this additional information is often unavailable.

4. Conclusions

The following conclusions can be drawn from the permeation results for SAPO-34 and MFI membranes presented in this paper:

(1) Binary Ar/CH_4 mixture permeation across SAPO-34 membrane is adequately modeled by the Habgood model, assuming uncoupled diffusion on individual species in the mixture. There is neither a significant slowing-down of Ar, nor a speeding-up of CH_4.
(2) For permeation of CO_2/H_2 mixture across SAPO-34 membrane the Habgood model does not anticipate correctly the slowing-down of the more mobile H_2. This slowing-down effect is over-emphasized by inclusion of the Vignes interpolated value for $Đ_{12}$ in the M–S equation (1).
(3) Slowing-down effects are quantified by the denominator terms in Eq. (6). Speeding-up effects are quantified by the cross-terms Δ_{ij}; however, the speeding-up effect is significant only when the more mobile species is also more strongly adsorbed.
(4) For permeation of CO_2/CH_4 mixture across MFI membrane there is both speeding-up of CO_2 and slowing-down of CH_4; the use of Vignes formula for $Đ_{12}$ under emphasizes both these effects.

Our study has highlighted the inadequacy of the Vignes interpolation formula for $Đ_{12}$ in providing a quantitatively correct description of slowing-down and speeding-up effects in zeolite diffusion. There is need for development of a better estimation procedure for $Đ_{12}$ that can be used in practice. This is the focus of our current ongoing research.

Acknowledgements

The Boulder group gratefully acknowledges support by the National Science Foundation, CTS-0413027 and Shell Global Solutions. RK acknowledges the grant of a TOP subsidy from The Netherlands Foundation for Fundamental Research (NWO-CW) for intensification of reactors.

Appendix A. Supplementary data

Supplementary data associated with this article can be found, in the online version, at doi:10.1016/j.seppur.2007.08.012.

References

[1] T. Tomita, K. Nakayama, H. Sakai, Gas separation characteristics of DDR type zeolite membrane, Micropor. Mesopor. Mater. 68 (2004) 71–75.
[2] R. Krishna, J.M. van Baten, Using molecular simulations for screening of zeolites for separation of CO_2/CH_4 mixtures, Chem. Eng. J. 133 (2007) 121–131.
[3] S. Li, J.L. Falconer, R.D. Noble, R. Krishna, Interpreting unary, binary and ternary mixture permeation across a SAPO-34 membrane with loading-dependent Maxwell–Stefan diffusivities, J. Phys. Chem. C 111 (2007) 5075–5082.
[4] R. Krishna, J.M. van Baten, Diffusion of alkane mixtures in zeolites. Validating the Maxwell–Stefan formulation using MD simulations, J. Phys. Chem. B 109 (2005) 6386–6396.
[5] J.M. van Baten, R. Krishna, Entropy effects in adsorption and diffusion of alkane isomers in mordenite: an investigation using CBMC and MD simulations, Micropor. Mesopor. Mater. 84 (2005) 179–191.
[6] R. Krishna, J.M. van Baten, A molecular dynamics investigation of diffusion of methane–ethane and methane–propane mixtures in zeolites, Chem. Eng. Technol. 29 (2006) 1429–1437.
[7] R. Krishna, J.M. van Baten, Diffusion of alkane mixtures in MFI zeolite, Micropor. Mesopor. Mater. 107 (2008) 296–298.
[8] R. Krishna, J.M. van Baten, Insights into diffusion of gases in zeolites gained from molecular dynamics simulations, Micropor. Mesopor. Mater. 109 (2008) 91–108.
[9] R. Krishna, R. Baur, Modelling issues in zeolite based separation processes, Sep. Purif. Technol. 33 (2003) 213–254.
[10] R. Krishna, Problems and pitfalls in the use of the fick formulation for intraparticle diffusion, Chem. Eng. Sci. 48 (1993) 845–861.
[11] R. Krishna, J.M. van Baten, E. García-Pérez, S. Calero, Incorporating the loading dependence of the Maxwell–Stefan diffusivity in the modeling of CH_4 and CO_2 permeation across zeolite membranes, Ind. Eng. Chem. Res. 46 (2007) 2974–2986.
[12] A.L. Myers, J.M. Prausnitz, Thermodynamics of mixed gas adsorption, AIChE J. 11 (1965) 121–130.
[13] R. Krishna, J.M. van Baten, E. García-Pérez, S. Calero, Diffusion of CH_4 and CO_2 in MFI, CHA and DDR zeolites, Chem. Phys. Lett. 429 (2006) 219–224.
[14] H.W. Habgood, The kinetics of molecular sieve action. Sorption of nitrogen–methane mixtures by Linde molecular sieve 4A, Can. J. Chem. 36 (1958) 1384–1397.
[15] R. Krishna, R. Baur, Diffusion, Adsorption and Reaction in Zeolites: Modelling and Numerical Issues, University of Amsterdam, Amsterdam, November 11, 2004, http://www.science.uva.nl/research/cr/zeolite/.
[16] M. Yu, J.L. Falconer, R.D. Noble, R. Krishna, Modeling transient permeation of polar organic mixtures through a MFI zeolite membrane using the Maxwell–Stefan equations, J. Membr. Sci. 293 (2007) 167–173.
[17] A.I. Skoulidas, D.S. Sholl, R. Krishna, Correlation effects in diffusion of CH_4/CF_4 mixtures in MFI zeolite. A study linking MD simulations with the Maxwell–Stefan formulation, Langmuir 19 (2003) 7977–7988.

Supplementary data to accompany:

Investigation of slowing-down and speeding-up effects in binary mixture permeation across SAPO-34 and MFI membranes

R. Krishna [a*], Shiguang Li [b], Jasper M. van Baten [a], John L. Falconer [b], Richard D. Noble [b]

[a] Van 't Hoff Institute for Molecular Sciences, University of Amsterdam, Nieuwe Achtergracht 166, 1018 WV Amsterdam, The Netherlands.

[b] Department of Chemical and Biological Engineering, University of Colorado Boulder, CO 80309-0424, U.S.A.

* Corresponding author. Tel: + 31 20 5257007; Fax: + 31 20 5255604; email address: r.krishna@uva.nl

Appendix A1. presents unary and binary permeation data for SAPO-34 and MFI membranes.

Appendix A1

Unary and Binary Permeation data in SAPO-34 and MFI membranes

SAPO-34 membrane permeation

Figure 1 shows a schematic of the membrane set-up. In our earlier publications [1, 2] we had reported data for permeation of unary gases (CO_2, CH_4, O_2, N_2, CO, H_2, He, and Ar) across a SAPO-34 membrane. The unary transport coefficients $\frac{\rho Đ_i}{\delta}$ for CO_2, CH_4, O_2, N_2, CO, H_2, He, and Ar were backed out from

$$\frac{\rho Đ_i}{\delta} = \frac{N_i}{DF_i} \tag{1}$$

using the procedure that has been described earlier[1]. These pure component transport coefficients are presented in Figure 2 as a function of the loadings at the upstream face of the membrane. For backing out these transport coefficients, $\frac{\rho Đ_i}{\delta}$, the statistical isotherm of Ruthven was used as described in our earlier work [1]

$$q_i = \frac{q_{i,sat}}{\Omega_i} \frac{b_i f_i + \sum_{m=2}^{\Omega_i} \frac{(b_i f_i)^m}{(m-1)!} \left[\frac{1 - \frac{m}{\Omega_i + 1}}{1 - \frac{1}{\Omega_i + 1}} \right]^m}{1 + b_i f_i + \sum_{m=2}^{\Omega_i} \frac{(b_i f_i)^m}{(m)!} \left[\frac{1 - \frac{m}{\Omega_i + 1}}{1 - \frac{1}{\Omega_i + 1}} \right]^m} \tag{2}$$

In eq (2), q_i represents the loading in mol kg^{-1}, $q_{i,sat}$ is the saturation loading, and Ω_i is maximum capacity expressed in molecules per cage. Based on the atomic composition of SAPO-34 used in our experiments, $(Si_{0.061}Al_{0.483}P_{0.455})O_2$, we calculate

$$q_{i,sat} = 1.369\Omega_i \tag{3}$$

Table 1 summarizes the values of the fit parameter b_i in eq. (2).

The loading dependence of the unary transport coefficients were described by the Reed and Ehrlich model

$$Đ_i = Đ_i(0)\frac{(1+\varepsilon_i)^{z-1}}{(1+\varepsilon_i/\phi_i)^z} \tag{4}$$

with

$$\varepsilon_i = \frac{(\beta_i - 1 + 2\theta_i)\phi_i}{2(1-\theta_i)}; \quad \beta_i = \sqrt{1 - 4\,\theta_i(1-\theta_i)(1-1/\phi_i)}; \quad \theta_i = \frac{q_i}{q_{i,sat}} \tag{5}$$

The fitted parameter values for z and ϕ_i are listed in Table 2 along with the corresponding zero-loading transport coefficients $\rho Đ_i(0)/\delta$..

Also presented in the earlier publication [1] were permeation data for binary gaseous mixtures (CO_2/CH_4, CO_2/N_2, N_2/CH_4, CH_4/H_2, CO/H_2 and N_2/H_2) across the SAPO-34 membrane. Additional experiments were carried out with the same membrane for the binary mixtures CO_2/H_2 and Ar/CH_4; the new experimental data are reported in Tables 3 and 4. The permeation fluxes for the set of eight binary mixtures (including six sets of earlier published data, along with the two new sets for CO_2/H_2 and Ar/CH_4) are summarized in Figure 3. Figure 4 presents the same data set plotted versus the total mixture loading at the upstream face of the membrane, q_{up}. The continuous solid lines in Figures 3 and 4 are the calculations obtained by numerical integration of the set of *uncoupled* Maxwell-Stefan equations, i.e. assuming that the binary exchange coefficients $Đ_{ij}$ are all infinite in value:

$$N_i = -\rho Đ_i \frac{q_i}{RT}\frac{d\mu_i}{dx}; \quad i = 1,...n \tag{6}$$

Equation (6) corresponds to the Habgood model for zeolite diffusion [3]. In these calculations, the Reed and Ehrlich model was used to describe the loading dependence of $\frac{\rho Đ_i}{\delta}$. In applying eq (4) to binary mixtures, total occupancy of the mixture was used

$$\theta = \frac{q_1}{q_{1,sat}} + \frac{q_2}{q_{2,sat}} \tag{7}$$

The ideal adsorbed solution theory (IAST) of Myers and Prausnitz [4] was used to calculate the component loadings in the mixture.

For the eight sets of *binary* permeation experiments we can back out the transport diffusivity $\rho Đ_i/\delta$ as a function of the total upstream loading, $q_{up} = q_{1,up} + q_{2,up}$; these results are presented in Figures 5a-h along with the values of unary transport coefficients for the eight binary mixture permeation experiments using

$$\frac{\rho Đ_i}{\delta} = \frac{N_i}{\int\limits_{upstream}^{downstream} \sum\limits_{j=1}^{n} \left(\Gamma_{ij} \frac{dq_j}{dx} \right) dx}; \quad i = 1,...n \tag{8}$$

It must be emphasized that the backed-out transport diffusivities $\rho Đ_i/\delta$ are *effective* parameters that will correspond with those obtained from unary experiments only when the exchange coefficients $Đ_{12}$ and $Đ_{21}$ in the M-S equations are infinite in value.

The transport coefficients of each of the six species (a) CH_4, (b) H_2, (c) Ar, (d) CO_2, (e) N_2, and (f) CO, both as pure components and in the eight mixtures investigated are summarized in Figure 6.

MFI membrane permeation

We also performed permeation experiments for pure component CO_2, CH_4, along with binary CO_2/CH_4 across an MFI (silicalite-1) membrane using the same set up as for the SAPO-34 membrane and shown in Figure 1. The membrane synthesis procedure, along with the experimental details are given below.

MFI Membrane Synthesis

The Silicalite-1 membrane was synthesized by in-situ crystallization on porous stainless steel tubes (0.8-μm pores, Pall Corp.). Non-porous, stainless steel tubes were welded onto each end of supports. The permeate area was approximately 7.8 cm^2. Before synthesis, the supports were boiled in distilled water for 1 h and dried at 373 K under vacuum for 30 min. The synthesis gel composition was 1 TPAOH: 19.5 SiO_2: 438 H_2O. The stainless steel tube with their outside wrapped in Teflon tape, was placed in an autoclave, which was then filled with synthesis gel. Three hydrothermal synthesis steps were applied. The first synthesis was carried at 458 K for about 48 h, whereas the second and third synthesis steps were each conducted at 458 K for 24 h using the same procedure. After each synthesis, the membrane was washed with distilled water at 293 K and dried at 373 K in a vacuum oven for 1 h. To remove the TPAOH template from the zeolite framework, the membrane was calcined in air at 673 K for 8 h. The heating and cooling rates were 0.7 and 0.9 K/min, respectively.

MFI Permeation experiments

Unary and binary mixture permeations were measured in the flow system described previously [1]; the system was modified to operate up to 7.2 MPa pressure. The membrane was mounted in a stainless steel module and sealed at each end with silicone o-rings. The pressure on each side of the membrane was independently controlled. Unary and mixture permeations were investigated as functions of feed pressure while maintaining a constant permeate pressure of 84 kPa. Fluxes were measured using a soap film bubble flow meter. The system was leak checked by replacing the membrane with a solid stainless steel tube. The leak rate for a 7 MPa pressure drop across the O-ring was below the detection limit of 1 $\times 10^{-14}$ mol m^{-2} s^{-1} Pa^{-1}.

The compositions of the feed, retentate, and permeate streams were measured online using a SRI 8610 C GC gas chromatograph equipped with a thermal conductivity detector and HAYESEP-D column (Alltech). The oven, injector, and detector temperatures were all kept at 423 K.

MFI Permeation data

The experimental data for unary permeation of CO_2 and CH_4 are presented in Tables 5, and 6. The binary permeation data for CO_2/CH_4 mixtures are summarized in Tables **7**. The binary CO_2/CH_4 mixture permeation fluxes across MFI membrane are plotted in Figure 7 as function of the upstream total pressure, f_{up}. The continuous solid lines represent the calculations by numerical solution of eq (6). For these predictions, the GCMC (Grand Canonical Monte Carlo) simulated pure component isotherms for CO_2 and CH_4 were fitted with a 3-site Langmuir isotherm, with parameters as listed in Table 8; these results are the based on our earlier work[5]. The Ideal Adsorbed Solution Theory (IAST) of Myers and Prausnitz [4] was used for calculation of mixture adsorption equilibrium. Figure 8 presents a comparison of transport coefficients, $\rho Đ_i/\delta$, for MFI membrane backed out from unary permeation and binary mixtures containing CO_2/CH_4. For the binary mixture experiments the $\rho Đ_i/\delta$ were backed out using eq. (8).

Literature cited

[1] S. Li, J.L. Falconer, R.D. Noble, R. Krishna, Interpreting unary, binary and ternary mixture permeation across a SAPO-34 membrane with loading-dependent Maxwell-Stefan diffusivities, J. Phys. Chem. C 111 (2007) 5075-5082.

[2] S. Li, J.L. Falconer, R.D. Noble, R. Krishna, Modeling permeation of CO_2/CH_4, CO_2/N_2, and N_2/CH_4 mixtures across SAPO-34 membrane with the Maxwell-Stefan equations, Ind. Eng. Chem. Res. 46 (2007) 3904-3911.

[3] H.W. Habgood, The kinetics of molecular sieve action. Sorption of nitrogen-methane mixtures by Linde molecular sieve 4A, Canad. J. Chem. 36 (1958) 1384-1397.

[4] A.L. Myers, J.M. Prausnitz, Thermodynamics of mixed gas adsorption, A.I.Ch.E.J. 11 (1965) 121-130.

[5] R. Krishna, J.M. van Baten, E. García-Pérez, S. Calero, Incorporating the loading dependence of the Maxwell-Stefan diffusivity in the modeling of CH_4 and CO_2 permeation across zeolite membranes, Ind. Eng. Chem. Res. 46 (2007) 2974-2986.

Table 1. Pure component isotherm fit data using eq (2).

Molecule	b_i	Ω_i	$q_{i,sat}$
CO_2	7.67×10^{-5}	6	8.2
CH_4	5.87×10^{-6}	6	8.2
N_2	1.26×10^{-6}	6	8.2
H_2	2.84×10^{-7}	9	12.3
O_2	1.2×10^{-6}	6	8.2
CO	2.31×10^{-6}	6	8.2
Ar	1.26×10^{-6}	6	8.2

b_i is expressed in Pa^{-1}, Ω_i in molecules per cage, $q_{i,sat}$ in mol kg^{-1}.

Table 2. Reed-Ehrlich parameters in various zeolite structures. Please note that this value of ϕ_1 for Ar is 2.3 and not 2.0 as erroneously listed in our earlier publication[1].

Molecule	$\rho \text{Đ}_i(0)/\delta$	Reed-Ehrlich model parameters in Eq (4) and (5)	
		z	ϕ_1
He	0.322	-	-
H_2	0.293	-	-
CO_2	4.6×10^{-3}	5	2.1
CH_4	3.2×10^{-4}	5	3
N_2	1.07×10^{-2}	5	2.3
O_2	2.53×10^{-2}	5	1.8
CO	1.14×10^{-2}	5	2
Ar	1.37×10^{-2}	5	2.3

Table 3. Binary CO_2-H_2 permeation data across SAPO-34 membrane.

upstream total pressure f_{up}	CO_2 upstream partial pressure $f_{1,up}$	H_2 upstream partial pressure $f_{2,up}$	CO_2 downstream partial pressure $f_{1,down}$	H_2 downstream partial pressure $f_{2,down}$	CO_2 flux N_1	H_2 flux N_2
0.77	0.37	0.40	0.07602	0.00798	0.07345	0.00771
2.15	0.97	1.18	0.07661	0.00739	0.14051	0.01356
3.51	1.52	1.99	0.07747	0.00653	0.17919	0.01510
4.87	2.05	2.82	0.07854	0.00546	0.19929	0.01385

$f_{i,up}$ and $f_{i,down}$ have the units MPa, N_i are expressed in mol m^{-2} s^{-1}

Table 4. Binary Ar - CH_4 permeation data across SAPO-34 membrane.

upstream total pressure f_{up}	Ar upstream partial pressure $f_{1,up}$	CH_4 upstream partial pressure $f_{2,up}$	Ar downstream partial pressure $f_{1,down}$	CH_4 downstream partial pressure $f_{2,down}$	Ar flux N_1	CH_4 flux N_2
0.43	0.21	0.21	0.0704	0.0136	0.00408	0.00079
0.77	0.39	0.39	0.0706	0.0134	0.00806	0.00153
1.46	0.73	0.74	0.0702	0.0138	0.01438	0.00283
2.50	1.24	1.26	0.0694	0.0146	0.02230	0.00467
3.53	1.74	1.79	0.0687	0.0153	0.03035	0.00674
4.91	2.41	2.50	0.0678	0.0162	0.03877	0.00923

$f_{i,up}$ and $f_{i,down}$ have the units MPa, N_i are expressed in mol m^{-2} s^{-1}

Table 5. Unary CO_2 permeation data for MFI membrane.

Upstream pressure, $f_{i,up}$	Downstream pressure, $f_{i,down}$	CO_2 flux, N_i
0.09	0.084	0.0029
0.12	0.084	0.0078
0.19	0.084	0.0160
0.24	0.084	0.0231
0.31	0.084	0.0312
0.43	0.084	0.0406
0.77	0.084	0.0627
1.46	0.084	0.0923
2.15	0.084	0.1109
2.84	0.084	0.1258
3.53	0.084	0.1394
4.22	0.084	0.1546
4.91	0.084	0.1708
5.60	0.084	0.1901

$f_{i,up}$ and $f_{i,down}$ have the units MPa, N_i are expressed in mol m^{-2} s^{-1}

Table 6. Unary CH_4 permeation data for MFI membrane.

Upstream pressure, $f_{i,up}$	Downstream pressure, $f_{i,down}$	CH_4 flux, N_i
0.11	0.084	0.0094
0.15	0.084	0.0183
0.22	0.084	0.0380
0.43	0.084	0.0840
0.77	0.084	0.1437
1.46	0.084	0.2252
2.15	0.084	0.2819
2.84	0.084	0.3320
3.53	0.084	0.3674
4.23	0.084	0.3992
4.92	0.084	0.4369
5.62	0.084	0.4659
6.33	0.084	0.5012
7.08	0.084	0.5387

$f_{i,up}$ and $f_{i,down}$ have the units MPa, N_i are expressed in mol m^{-2} s^{-1}

Table 7. Binary CO_2-CH_4 permeation data for MFI membrane. The feed composition was approximately 50% : 50%.

Total upstream pressure f_{up}	CO_2 upstream partial pressure $f_{1,up}$	CH_4 upstream partial pressure $f_{2,up}$	CO_2 downstream partial pressure $f_{1,down}$	CH_4 downstream partial pressure $f_{2,down}$	CO_2 flux N_1	CH_4 flux N_2
0.77	0.38	0.39	0.060	0.0236	0.0434	0.0170
1.46	0.71	0.75	0.059	0.0251	0.0664	0.0283
2.15	1.04	1.11	0.057	0.0266	0.0912	0.0422
2.84	1.36	1.48	0.056	0.0275	0.1154	0.0562
3.53	1.67	1.86	0.056	0.0282	0.1350	0.0684
4.22	1.98	2.23	0.055	0.0290	0.1522	0.0802
4.98	2.33	2.65	0.054	0.0298	0.1671	0.0918
5.93	2.76	3.18	0.053	0.0307	0.1847	0.1066

$f_{i,up}$ and $f_{i,down}$ have the units MPa, N_i are expressed in mol m^{-2} s^{-1}

Table 8. Three-site Langmuir parameters for CH_4 and CO_2 in MFI. The saturation capacity q_{sat} has the units of mol kg^{-1}. The Langmuir parameters b_i, have the units of Pa^{-1}.

Zeolite	Molecule, Temperature	Three-Site Langmuir parameters					
		$b_{i,A}$	$q_{i,sat,A}$	$b_{i,B}$	$q_{i,sat,B}$	$b_{i,C}$	$q_{i,sat,C}$
MFI	CH_4, 300 K	3.25×10^{-6}	2.8	2.2×10^{-8}	0.7	1.12×10^{-10}	0.5
MFI	CO_2, 300 K	5.78×10^{-6}	3.4	2.76×10^{-8}	1.0	1.46×10^{-9}	1.5

Captions for Figures

Figure 1. Schematic of membrane set-up used for SAPO-34 and MFI membrane.

Figure 2. Pure component transport coefficients, $\rho Đ_i/\delta$, for (a) He, H_2, (b) CO_2, N_2, O_2, Ar, and (c) CH_4 for transport across SAPO-34 membrane backed out using eq (1).

Figure 3. Permeation fluxes for binary (a) CO_2/CH_4, (b) CO_2/N_2, (c) N_2/CH_4, Ar/CH_4 (e) CH_4/H_2, (f) N_2/H_2, (g) CO/H_2, and (h) CO_2/H_2 and mixtures across SAPO-34 membrane as function of the upstream total pressure, f_{up}. The continuous solid lines represent the calculations by numerical solution of eq (6).

Figure 4. Permeation fluxes for binary (a) CO_2/CH_4, (b) CO_2/N_2, (c) N_2/CH_4, Ar/CH_4 (e) CH_4/H_2, (f) N_2/H_2, (g) CO/H_2, and (h) CO_2/H_2 mixtures across SAPO-34 membrane as function of total mixture loading at the upstream face of the membrane, q_{up}. The continuous solid lines represent the calculations by numerical solution of eq (6).

Figure 5. Comparison of transport coefficients, $\rho Đ_i/\delta$, for SAPO-34 membrane backed out from unary permeation and binary mixtures containing (a) CO_2/CH_4, (b) CO_2/N_2, (c) N_2/CH_4, (d) Ar/CH_4 (e) CH_4/H_2, (f) N_2/H_2, (g) CO/H_2, and (h) CO_2/H_2.

Figure 6. Transport coefficients, $\rho Đ_i/\delta$, for SAPO-34 membrane backed out from unary permeation of (a) CH_4, (b) H_2, (c) Ar, (d) CO_2, (e) N_2, and (f) CO.

Figure 7. Permeation fluxes for binary CO_2/CH_4 mixture across MFI membrane as function of the upstream total pressure, f_{up}. The continuous and dashed solid lines represent the calculations by numerical solution of eq (6).

Figure 8. Comparison of transport coefficients, $\rho Đ_i/\delta$, for MFI membrane backed out from unary permeation and binary mixtures containing CO_2/CH_4.

Figure 1

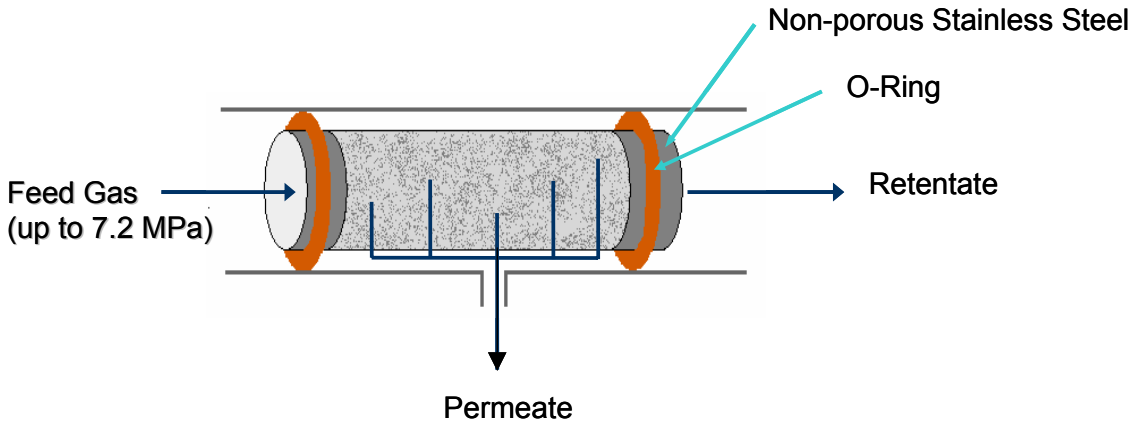
Non-porous Stainless Steel
O-Ring
Feed Gas
(up to 7.2 MPa)
Retentate
Permeate

Figure 2

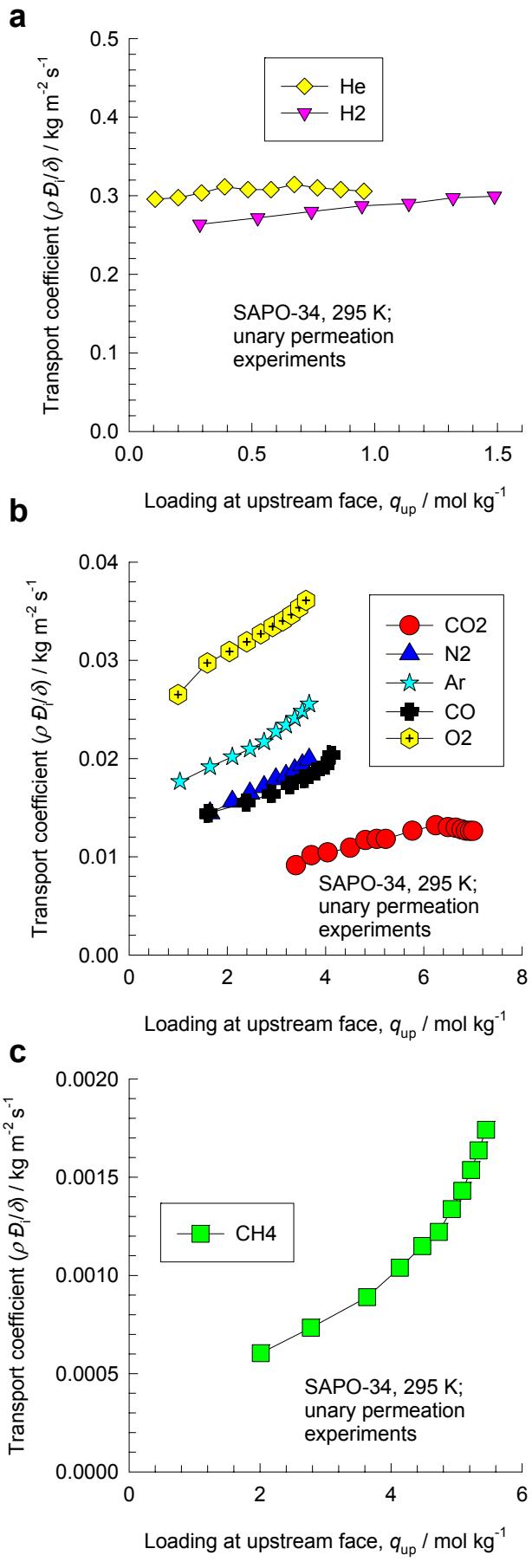
a
Transport coefficient ($\rho Đ_i/\delta$) / kg m^{-2} s^{-1}
0.0
0.1
0.2
0.3
0.4
0.5
He
H2
SAPO-34, 295 K;
unary permeation
experiments
0.0
0.5
1.0
1.5
Loading at upstream face, q_{up} / mol kg^{-1}
b
Transport coefficient ($\rho Đ_i/\delta$) / kg m^{-2} s^{-1}
0.00
0.01
0.02
0.03
0.04
CO2
N2
Ar
CO
O2
SAPO-34, 295 K;
unary permeation
experiments
0
2
4
6
8
Loading at upstream face, q_{up} / mol kg^{-1}
c
Transport coefficient ($\rho Đ_i/\delta$) / kg m^{-2} s^{-1}
0.0000
0.0005
0.0010
0.0015
0.0020
CH4
SAPO-34, 295 K;
unary permeation
experiments
0
2
4
6
Loading at upstream face, q_{up} / mol kg^{-1}

Figure 3

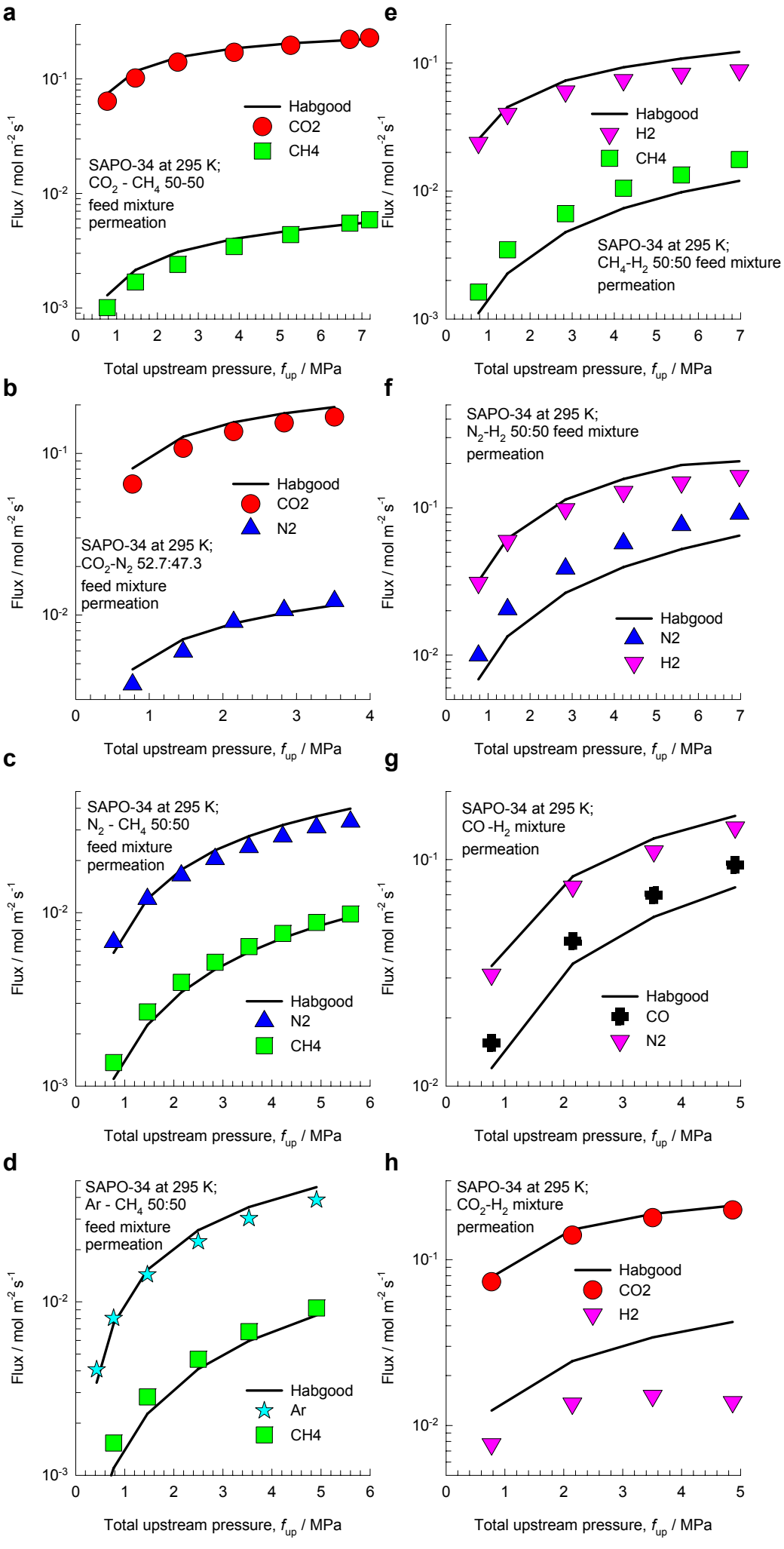
a
SAPO-34 at 295 K;
CO2 - CH4 50-50
feed mixture
permeation
Habgood
CO2
CH4
Flux / mol m-2 s-1
Total upstream pressure, fup / MPa
b
SAPO-34 at 295 K;
CO2-N2 52.7:47.3
feed mixture
permeation
Habgood
CO2
N2
c
SAPO-34 at 295 K;
N2 - CH4 50:50
feed mixture
permeation
Habgood
N2
CH4
d
SAPO-34 at 295 K;
Ar - CH4 50:50
feed mixture
permeation
Habgood
Ar
CH4
e
Habgood
H2
CH4
SAPO-34 at 295 K;
CH4-H2 50:50 feed mixture
permeation
f
SAPO-34 at 295 K;
N2-H2 50:50 feed mixture
permeation
Habgood
N2
H2
g
SAPO-34 at 295 K;
CO -H2 mixture
permeation
Habgood
CO
N2
h
SAPO-34 at 295 K;
CO2-H2 mixture
permeation
Habgood
CO2
H2

Figure 4

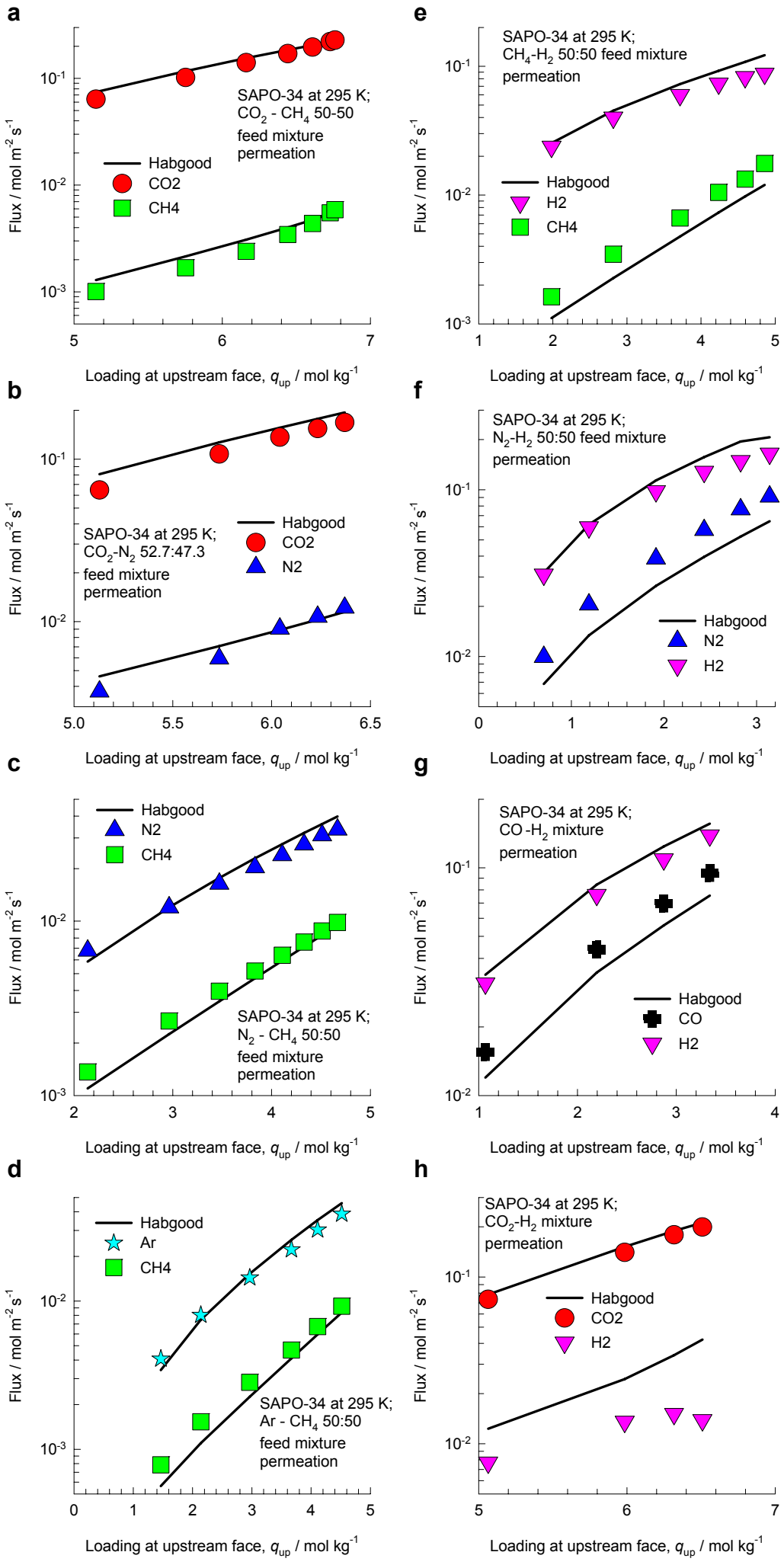
a
SAPO-34 at 295 K;
CO2 - CH4 50-50
feed mixture
permeation
Habgood
CO2
CH4
Flux / mol m-2 s-1
Loading at upstream face, qup / mol kg-1
b
SAPO-34 at 295 K;
CO2-N2 52.7:47.3
feed mixture
permeation
Habgood
CO2
N2
c
Habgood
N2
CH4
SAPO-34 at 295 K;
N2 - CH4 50:50
feed mixture
permeation
d
Habgood
Ar
CH4
SAPO-34 at 295 K;
Ar - CH4 50:50
feed mixture
permeation
e
SAPO-34 at 295 K;
CH4-H2 50:50 feed mixture
permeation
Habgood
H2
CH4
f
SAPO-34 at 295 K;
N2-H2 50:50 feed mixture
permeation
Habgood
N2
H2
g
SAPO-34 at 295 K;
CO -H2 mixture
permeation
Habgood
CO
H2
h
SAPO-34 at 295 K;
CO2-H2 mixture
permeation
Habgood
CO2
H2

Figure 5

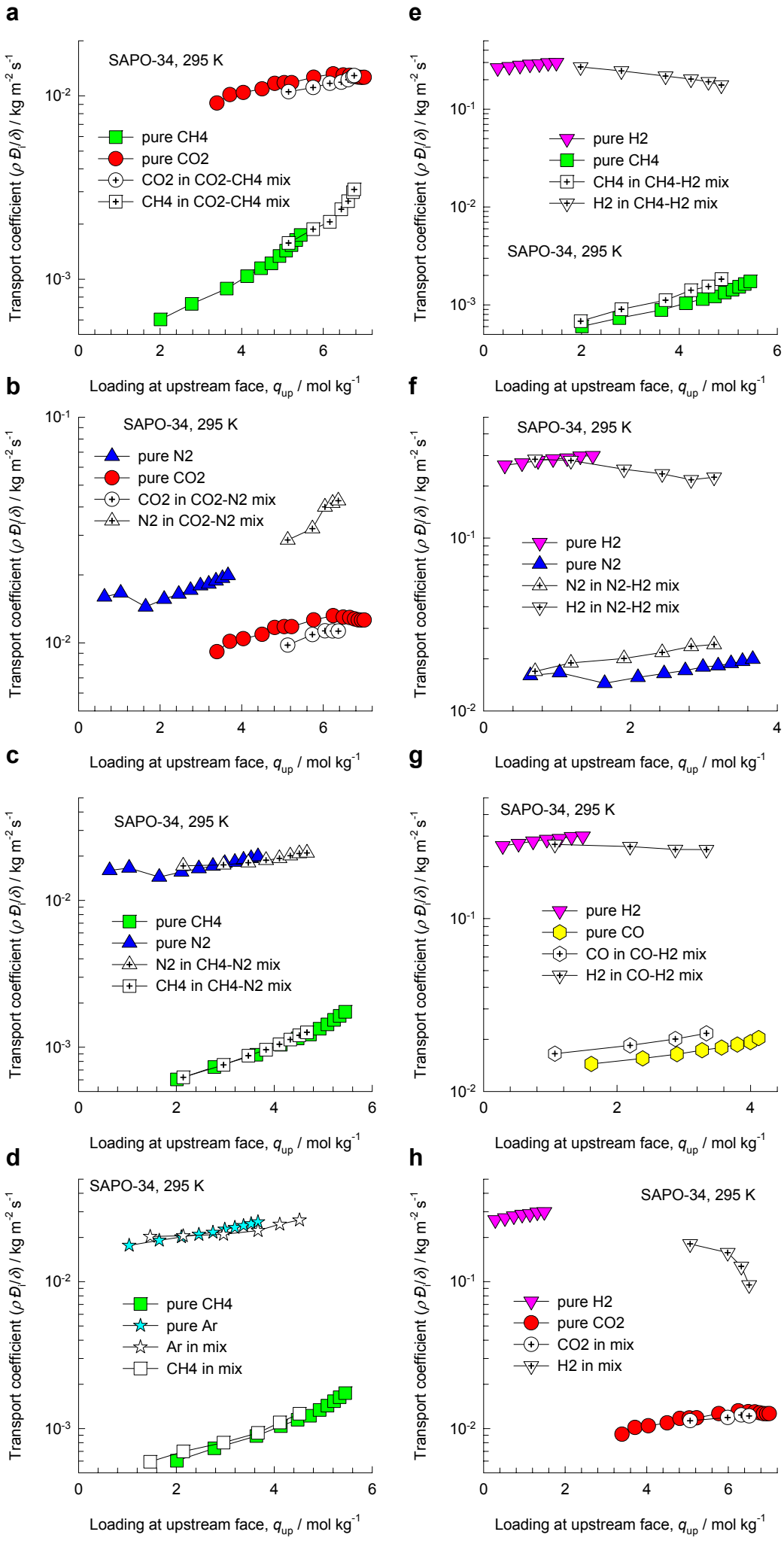
a
SAPO-34, 295 K
pure CH4
pure CO2
CO2 in CO2-CH4 mix
CH4 in CO2-CH4 mix
b
SAPO-34, 295 K
pure N2
pure CO2
CO2 in CO2-N2 mix
N2 in CO2-N2 mix
c
SAPO-34, 295 K
pure CH4
pure N2
N2 in CH4-N2 mix
CH4 in CH4-N2 mix
d
SAPO-34, 295 K
pure CH4
pure Ar
Ar in mix
CH4 in mix
e
pure H2
pure CH4
CH4 in CH4-H2 mix
H2 in CH4-H2 mix
SAPO-34, 295 K
f
SAPO-34, 295 K
pure H2
pure N2
N2 in N2-H2 mix
H2 in N2-H2 mix
g
SAPO-34, 295 K
pure H2
pure CO
CO in CO-H2 mix
H2 in CO-H2 mix
h
SAPO-34, 295 K
pure H2
pure CO2
CO2 in mix
H2 in mix
Transport coefficient ($\rho Đ_i/\delta$) / kg m^{-2} s^{-1}
Loading at upstream face, q_{up} / mol kg^{-1}

Figure 6

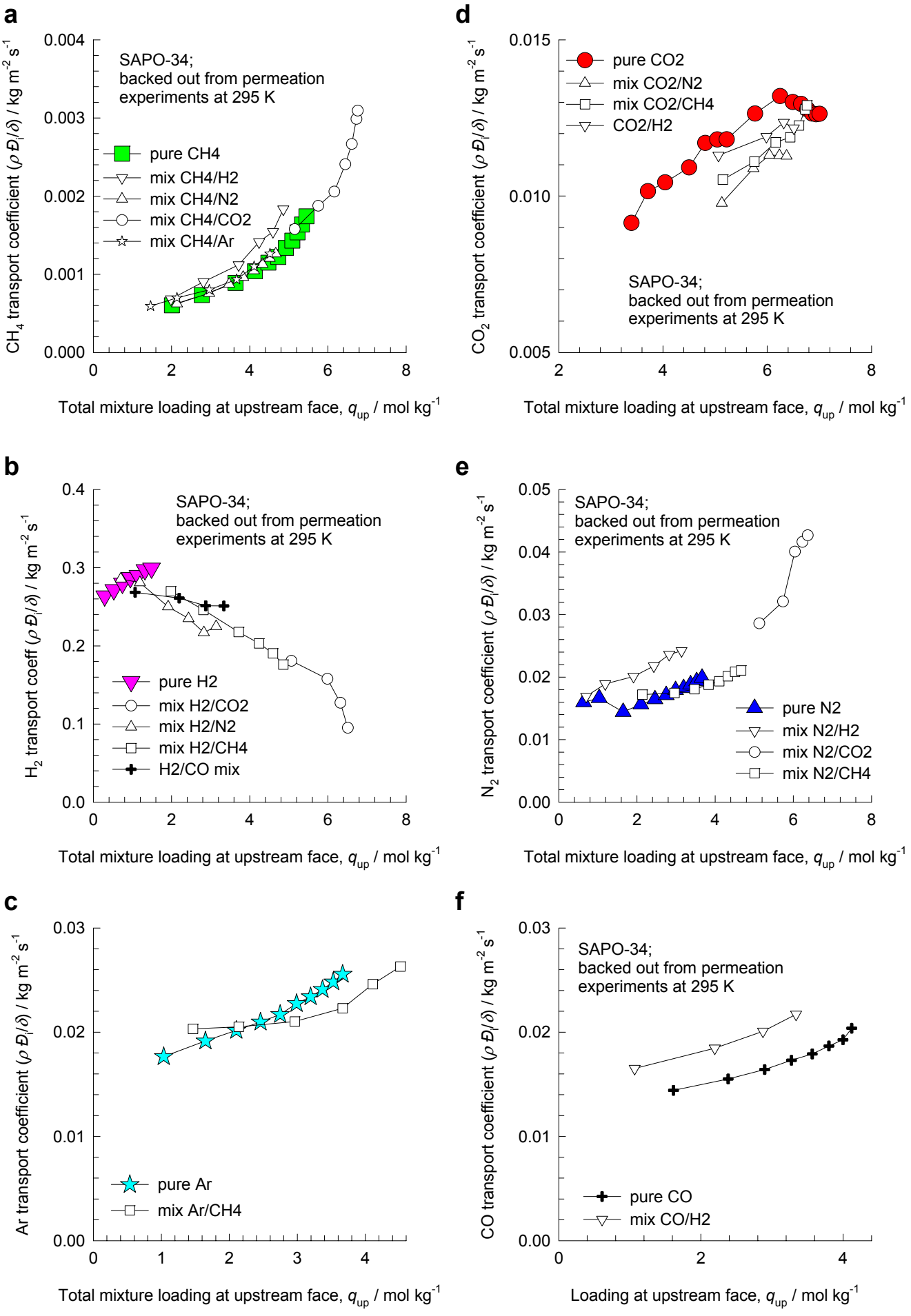
a
SAPO-34;
backed out from permeation
experiments at 295 K
pure CH4
mix CH4/H2
mix CH4/N2
mix CH4/CO2
mix CH4/Ar
CH4 transport coefficient (ρ Đi/δ) / kg m-2 s-1
Total mixture loading at upstream face, qup / mol kg-1
d
pure CO2
mix CO2/N2
mix CO2/CH4
CO2/H2
SAPO-34;
backed out from permeation
experiments at 295 K
CO2 transport coefficient (ρ Đi/δ) / kg m-2 s-1
Total mixture loading at upstream face, qup / mol kg-1
b
SAPO-34;
backed out from permeation
experiments at 295 K
pure H2
mix H2/CO2
mix H2/N2
mix H2/CH4
H2/CO mix
H2 transport coeff (ρ Đi/δ) / kg m-2 s-1
Total mixture loading at upstream face, qup / mol kg-1
e
SAPO-34;
backed out from permeation
experiments at 295 K
pure N2
mix N2/H2
mix N2/CO2
mix N2/CH4
N2 transport coefficient (ρ Đi/δ) / kg m-2 s-1
Total mixture loading at upstream face, qup / mol kg-1
c
pure Ar
mix Ar/CH4
Ar transport coefficient (ρ Đi/δ) / kg m-2 s-1
Total mixture loading at upstream face, qup / mol kg-1
f
SAPO-34;
backed out from permeation
experiments at 295 K
pure CO
mix CO/H2
CO transport coefficient (ρ Đi/δ) / kg m-2 s-1
Loading at upstream face, qup / mol kg-1

Figure 7

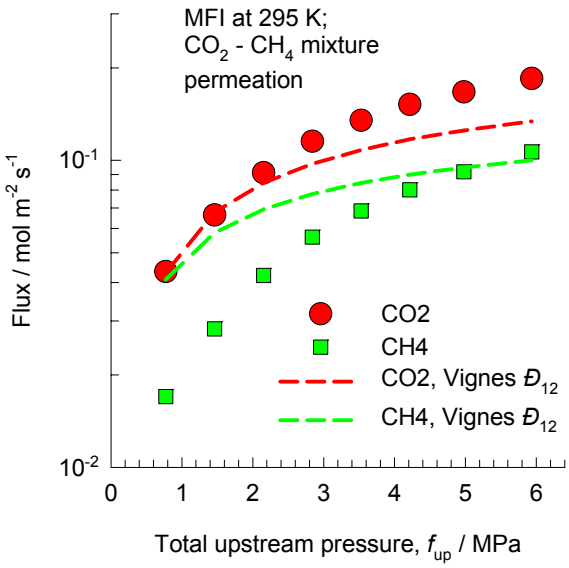
MFI at 295 K;
CO2 - CH4 mixture
permeation
CO2
CH4
CO2, Vignes Đ12
CH4, Vignes Đ12
Flux / mol m-2 s-1
10-1
10-2
0
1
2
3
4
5
6
Total upstream pressure, fup / MPa

Figure 8

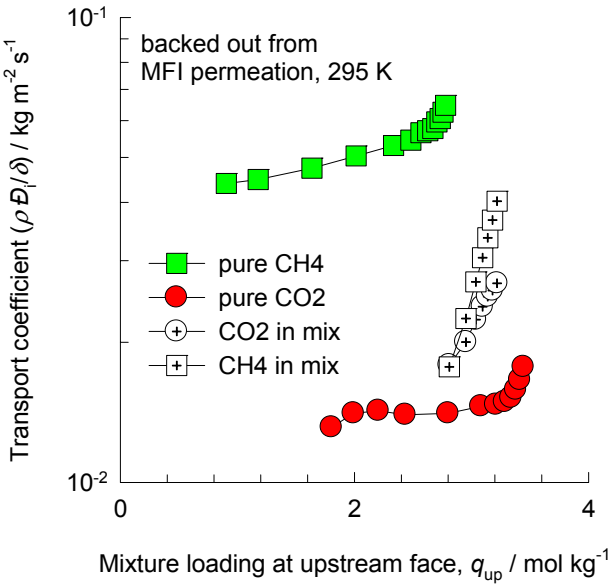
backed out from
MFI permeation, 295 K
pure CH4
pure CO2
CO2 in mix
CH4 in mix
Transport coefficient ($\rho Đ_i/\delta$) / kg m^{-2} s^{-1}
Mixture loading at upstream face, q_{up} / mol kg^{-1}
10^{-1}
10^{-2}
0
2
4